Non-universality of the Turbulent Spectra at Sub-ion Scales in the Solar Wind: Dispersive Effects versus the Doppler Shift

Fouad Sahraoui, Shiyong Huang

The Astrophysical Journal, 956:89 (7pp), 2023 October 20 https://doi.org/10.3847/1538-4357/acf45b

Non-universality of the Turbulent Spectra at Sub-ion Scales in the Solar Wind: Dispersive Effects versus the Doppler Shift

Fouad Sahraoui[1] and Shiyong Huang[2]
[1] Laboratoire de Physique des Plasmas, CNRS-Ecole Polytechnique-Sorbonne Université-Observatoire de Paris-Université Paris-Saclay, Route de Saclay, F-91128 Palaiseau, France; fouad.sahraoui@lpp.polytechnique.fr
[2] School of Electronic Information, Wuhan University, Wuhan, 430072, People's Republic of China
Received 2022 December 1; revised 2023 August 21; accepted 2023 August 25; published 2023 October 11

Abstract

Large surveys of the power spectral density of the magnetic fluctuations in the solar wind have reported different slope distributions at MHD, sub-ion and sub-electron scales: the smaller the scale, the broader the distribution. Here, we review briefly some of the most relevant explanations of the broadening of the slopes at sub-ion scales. Then, we present a new one that has been overlooked in the literature, which is based on the relative importance of the dispersive effects with respect to the Doppler shift due to the mean flow speed. We build a toy model based on a dispersion relation of a linear mode that matches at high frequency ($\omega \gtrsim \omega_{ci}$) the Alfvén (respectively whistler) mode at high oblique (respectively quasi-parallel) propagation angles $\theta_{\boldsymbol{kB}}$. Starting with a double power-law spectrum of turbulence ${k_\perp}^{-1.66}$ in the inertial range and ${k_\perp}^{-2.8}$ at the sub-ion scales, the transformed spectrum (in frequency f) as it would be measured in the spacecraft reference frame shows a broad range of slopes at the sub-ion scales that depend both on the angle $\theta_{\boldsymbol{kB}}$ and the flow speed V. Varying $\theta_{\boldsymbol{kB}}$ in the range 4°–106° and V in the range 400−800 km s^{-1} the resulting distribution of slopes at the sub-ion scales reproduces quite well the observed one in the solar wind. Fluctuations in the solar wind speed and the wavevector anisotropy of the turbulence may explain (or at least contribute to) the variability of the spectral slopes reported from spacecraft observations in the solar wind.

Unified Astronomy Thesaurus concepts: Interplanetary turbulence (830); Solar wind (1534)

1. Introduction

In situ measurements in near-Earth space from numerous orbiting spacecraft (e.g.,Wind, Helios, ACE, and Cluster) provided in-depth information about the nature of the plasma turbulence over a broad range of scales that span the MHD and the kinetic ranges. In the solar wind the power spectral density (PSD) of the magnetic fluctuations is shown to have at least four distinct ranges of scales separated by spectral breaks occurring near the proton and electron gyroradii (or inertial lengths). First is the energy-containing range observed in the fast solar wind that has a scaling $\sim f^{-1}$ for frequencies $\lesssim 10^{-4}$ Hz (given in the spacecraft reference frame; Bavassano et al. 1982). The origin of this range, also known as the energy driving scales or the "$1/f$ flicker noise," remains an open question (Matthaeus et al. 2007; Velli et al. 1989; Dmitruk & Matthaeus 2007; Verdini et al. 2012; Bruno & Carbone 2013; Chandran 2018; Matteini et al. 2018). The "*1/f* noise" spectrum is observed also in terrestrial and other planetary magnetosheaths (Tao et al. 2015; Hadid et al. 2015; Huang et al. 2017, 2020a), in the solar photospheric magnetic field (Matthaeus et al. 2007), in electronic devices, in dynamo experiments, and in geophysical flows (see Dmitruk et al. 2011 and the references therein). The $1/f$ spectrum is followed by the inertial range in the frequency range $\sim[10^{-4}, 10^{-1}]$ Hz where dissipation is negligible and the dynamics is controlled by the nonlinear interaction between counterpropagating Alfvén waves. The dominant scaling is $f^{-5/3}$, although the recent Parker Solar Probe (PSP) data revived the old debate as to whether the scaling in this range follows the Kolmogorov spectrum $k^{-5/3}$ or the Iroshnikov–Kraichnan prediction $k^{-3/2}$ (Iroshnikov 1963; Kraichnan 1965). This point will not be further discussed in this paper. At frequencies $\sim$[0.1, 1] Hz corresponding to characteristic ion scales a spectral break appears and the spectra can steepen significantly to $\sim f^{-4.5}$ over a narrow frequency band, which was termed the *transition range* in Sahraoui et al. (2010), but is often referred to as the dissipation range (Goldstein et al. 1994; Leamon et al. 1998; Stawicki et al. 2001; Smith et al. 2006; Bruno & Trenchi 2014). In the frequency range $\sim$[3, 30] Hz, which corresponds to the dispersive range far below the ion scale, a scaling f^{α} with $\alpha \in [-3.1, -2.3]$ is generally reported (Alexandrova et al. 2012; Sahraoui et al. 2013; Huang et al. 2021). In this range, the main focus of this work, dispersive and dissipation effects become important, and the nature of the turbulent fluctuations is still debated (He et al. 2011, 2012; Gary et al. 2012; Huang et al. 2020b), although the Kinetic Alfvén Waves (KAW) scenario seems to have won the battle (Bale et al. 2005; Sahraoui et al. 2009, 2010; He et al. 2011, 2012; Gary et al. 2012; Podesta & TenBarge 2012; Salem et al. 2012; Chen et al. 2013; Kiyani et al. 2013). At higher frequencies (typically $f \gtrsim 40$ Hz) corresponding to the electron scales, a new steepening of the magnetic energy spectra has been seen and interpreted as the onset of the electron dissipation range (Sahraoui et al. 2009). The actual scaling (power law versus exponential) of that range is still in question. This is due mainly to instrumental limitations (i.e., a weak signal-to-noise ratio) at those frequencies (Sahraoui et al. 2013; Dudok de Wit et al. 2022), which calls for more sensitive search-coil magnetometers and a dedicated space mission to resolve the nature of the electron dissipation range of solar wind turbulence (Verscharen et al. 2021).

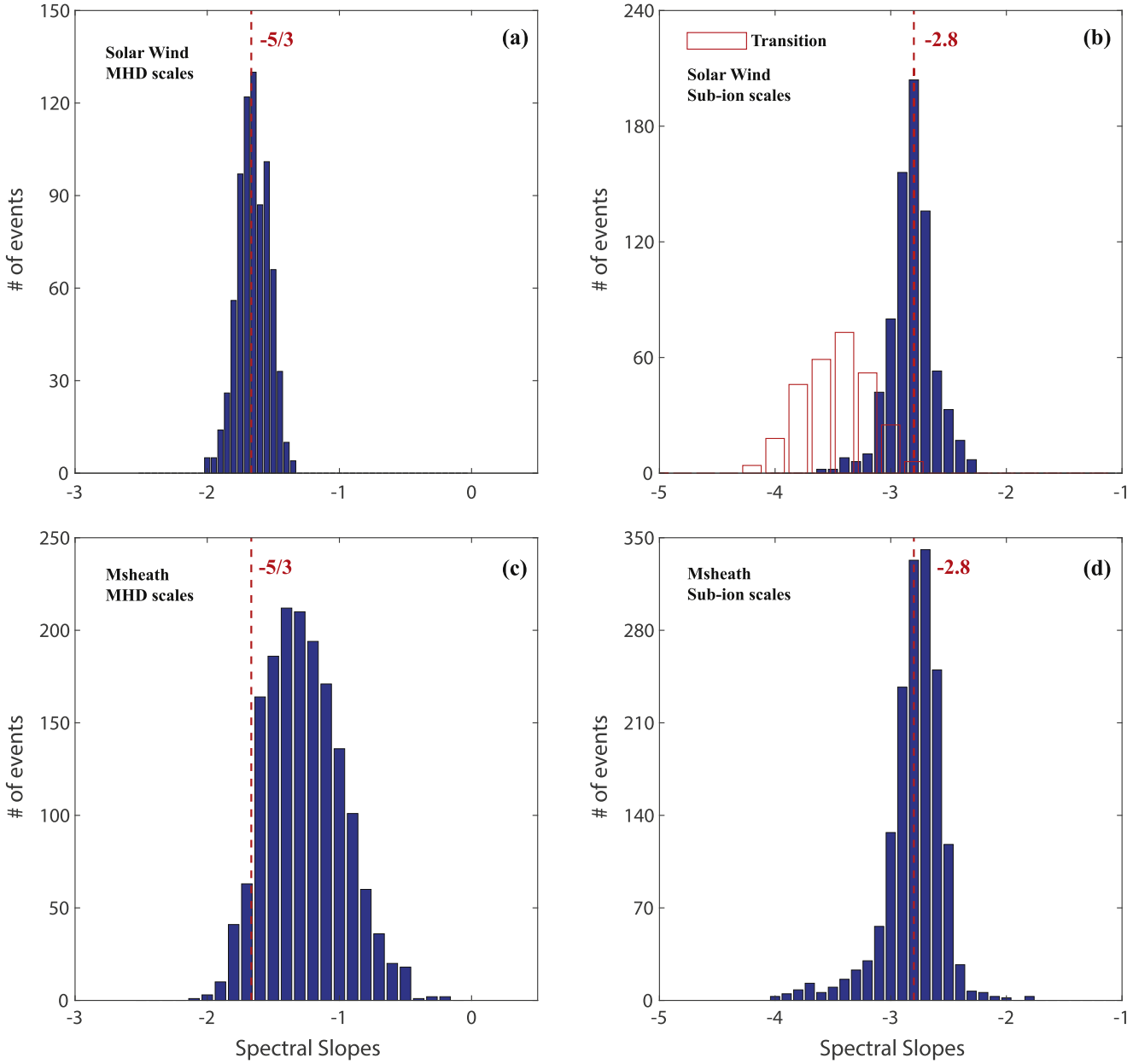

Figure 1. Distribution of spectral slopes in the inertial range and sub-ion scales of the solar wind (a and b) and magnetosheath (c and d) turbulence obtained from the Cluster spacecraft data. Figure adapted from Sahraoui et al. (2013) and Huang et al. (2014).

Large surveys of the slopes of the magnetic PSD in the solar wind have been conducted in the past years from various spacecraft data (Alexandrova et al. 2012; Sahraoui et al. 2013; Huang et al. 2021). An overview of the statistical results obtained both at MHD and sub-ion scales from the Cluster spacecraft data in the solar wind and the terrestrial magnetosheath are summarized in Figure 1. Two striking features can be seen. In the solar wind, the slopes are more spread at the sub-ion scales than in the inertial range. This may indicate the lack of universality of kinetic turbulence in comparison with the inertial range. However, the distribution of slopes in the dispersion range (excluding the transition range reflected by the histogram in Figure 1(b)) is very similar to that in the magnetosheath (Figure 1(d)), although the plasma conditions in the two regions are generally very different (Sahraoui et al. 2013; Huang et al. 2014, 2017). Furthermore, the slopes in that range were found not to depend either on the location within the magnetosheath or on the dynamics of the large scales boundaries, namely the shock and the magnetopause (Hadid et al. 2015; Huang et al. 2017). The magnetosheath results will not discussed further in this paper; the reader is referred to Hadid et al. (2015) and Huang et al. (2017) for a thorough analysis of turbulence properties in the magnetosheath.

Why the spectral slopes are more scattered on the sub-ion scales than they are in the inertial range? Is it evidence of a lack of universality of kinetic turbulence in comparison to MHD turbulence? Note that the spectral slopes at the sub-electron scales (not shown here) are even more scattered than those of Figures 1(b) and (d); (Sahraoui et al. 2013; Huang et al. 2014).

Before digging a bit more into these questions, one should first distinguish between the two ranges of the scales discussed above, the transition and the dispersive ranges. The steepening of spectra in the transition range has been reported in early observations in the solar wind at 1 au using the fluxgate

magnetometer data that covers the frequency band $\lesssim$3 Hz (the spectral break occurs at $f \sim 0.1$–0.5 Hz; Goldstein et al. 1994; Leamon et al. 1998; Bale et al. 2005; Smith et al. 2006), while the dispersive range has been explored relatively recently thanks to the high time resolution of the search-coil magnetometers data from the Cluster spacecraft (Sahraoui et al. 2009; Kiyani et al. 2009; Alexandrova et al. 2009) and from the even more recent PSP and Solar Orbiter data (Kretzschmar et al. 2021; Dudok de Wit et al. 2022). Several explanations of the steepening in the transition range have been proposed, but not all are consistent with, or directly linked to, each other. The physics of the transition range is indeed very complex because of, among other reasons, the presence of a variety of plasma instabilities that kick in near $k\rho_i \sim 1$ whose effects on the background turbulence are still poorly understood (Sahraoui et al. 2004, 2006; Kunz et al. 2014, 2018; Simon & Sahraoui 2022). In addition, theoretical predictions are generally obtained in asymptotic limits, typically $k\rho_i \ll 1$ or $k\rho_i \gg 1$ and $k\rho_e \ll 1$ (Schekochihin et al. 2009), which excludes that range. And numerical simulations either do not fully describe the kinetic physics in that range, e.g., hybrid or gyrokinetic codes (Howes et al. 2011; Parashar et al. 2011), or when they do (e.g., PIC codes) the simulations do not bear a realistic scale separation needed to capture the physics of the transition range (e.g., using an unrealistic proton-to-electron mass ratio, forcing the simulations near the ion or electron scales; Gary et al. 2012; Wan et al. 2012).

Some of the proposed explanations of the steepening in the transition range include damping of part of the turbulent fluctuations by either cyclotron resonance (Goldstein et al. 1994; Leamon et al. 1998; Bruno & Trenchi 2014; He et al. 2015) or Landau damping (Leamon et al. 1999; Sahraoui et al. 2010); a stronger energy dissipation rate estimated in the inertial range using the third-order law formalism of incompressible MHD turbulence (Smith et al. 2006; note that this explanation is related to the correlation found between large amplitude fluctuations in the inertial range and steeper spectra in the fast solar wind by Bruno et al. 2014); the dominance of the left-handed fluctuations (Meyrand & Galtier 2012; Huang et al. 2020b); the superposition of a high-frequency KAW cascade that has shallow spectra ($k_\perp{}^{-7/3}$) and a low-frequency ion-entropy cascade with steeper spectra ($k_\perp{}^{-16/5}$; Schekochihin et al. 2009); and the presence of a weakly dispersive regime of KAW turbulence (Voitenko & de Keyser 2011). Numerical simulations using the Landau-fluid code showed the slopes depend on the balance between the strength of nonlinear interactions (controlled by the parameter $\chi = \frac{k_\perp \delta B}{k_\parallel B_0}$) and that of collisionless Landau damping (Passot & Sulem 2015; Sulem et al. 2016; Kobayashi et al. 2017). Other explanations have been proposed more recently based on the imbalance, i.e., the high cross-helicity of the Alfvénic fluctuations (Passot & Sulem 2019) and the concept of a helicity barrier (Meyrand et al. 2021; Squire et al. 2022; Huang et al. 2022).

In the following, we will focus on the dispersive range that appears at higher frequencies than those of the transition range. In particular, we will propose an alternative explanation to the variability of the spectral slopes of the magnetic energy spectra as recalled by Figure 1 based on the balance between the dispersive and the Doppler shift due the mean solar wind flow.

2. Dispersion versus Doppler Shift: A Toy Model

The alternative explanation we present in this section is based on a key observational point that has been overlooked in the literature, namely the relative importance of the dispersive effects with respect to the Doppler shift. This problem is commonly referred to as the spatio-temporal ambiguity inherent to measurements made on board a single spacecraft. Indeed, the turbulence spectra are measured on board the spacecraft as function of the frequency. Each frequency ω_{sc} in that spectrum has two contributions, a temporal one that is the frequency of the fluctuation in the plasma rest frame ω_{plas}, and a spatial one due to the Doppler shift $\boldsymbol{k} \cdot \boldsymbol{V}$ ($\boldsymbol{k}$ being the wavevector of the fluctuation). These three quantities are related by the relation

$$\omega_{sc} = \omega_{plas} + \boldsymbol{k} \cdot \boldsymbol{V} = \omega_{plas} + kV \cos\theta_{\mathbf{kV}} \quad (1)$$

where $\theta_{\mathbf{kV}}$ is the angle between wavevector $\boldsymbol{k}$ and flow speed $\boldsymbol{V}$. Note that in this work, and as reflected by Equation (1), we do not consider the possible effect of sweeping of the small-scale fluctuations by large-scale ones.

To remove the spatio-temporal ambiguity, that is, the separate estimations the two terms of the right-hand side of Equation (1), multispacecraft data obtained simultaneously in various points in space and suitable analysis techniques (e.g., the k-filtering Sahraoui et al. 2006) are required. When only single spacecraft data are available, a partial solution to the problem (i.e., the estimation of one of the two right-hand-side terms of Equation (1)) is possible but at a cost of imposing additional assumptions. This is particularly the case for the so-called Taylor hypothesis widely used in solar wind studies. Indeed, considering the high flow speed ($V \sim 400$–800 km s^{-1}) with respect to the fluctuations speed ($V_A \sim 100$ km s^{-1}) the Taylor hypothesis neglects ω_{plas} next to $\boldsymbol{k} \cdot \boldsymbol{V}$ to infer the spectra in the wavenumber space from the frequency ones measured on board the spacecraft. More rigorously, the phase speeds of the fluctuations must be smaller than the flow speed *projected* onto the wavevector $\boldsymbol{k}$, as can be seen in Equation (1), and, under that (restrictive) condition, only one component of the wavevector (the one along the flow $\boldsymbol{V}$) can be inferred. While the Taylor hypothesis may hold at large (MHD)

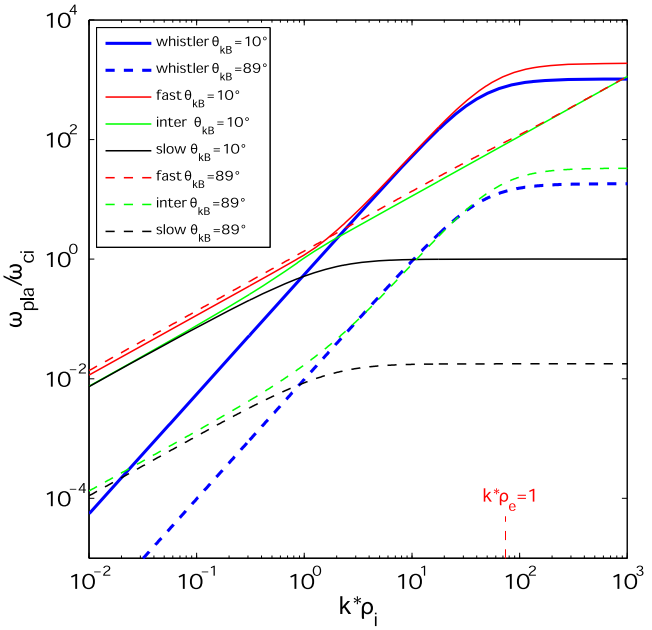

Figure 2. Numerical solutions of Equation (2) for quasi-parallel (solid blue) and quasi-perpendicular (dashed blue) propagation compared to the linear dispersion relations (slow, Alfvén or intermediate, and fast modes) computed using the two-fluid theory.

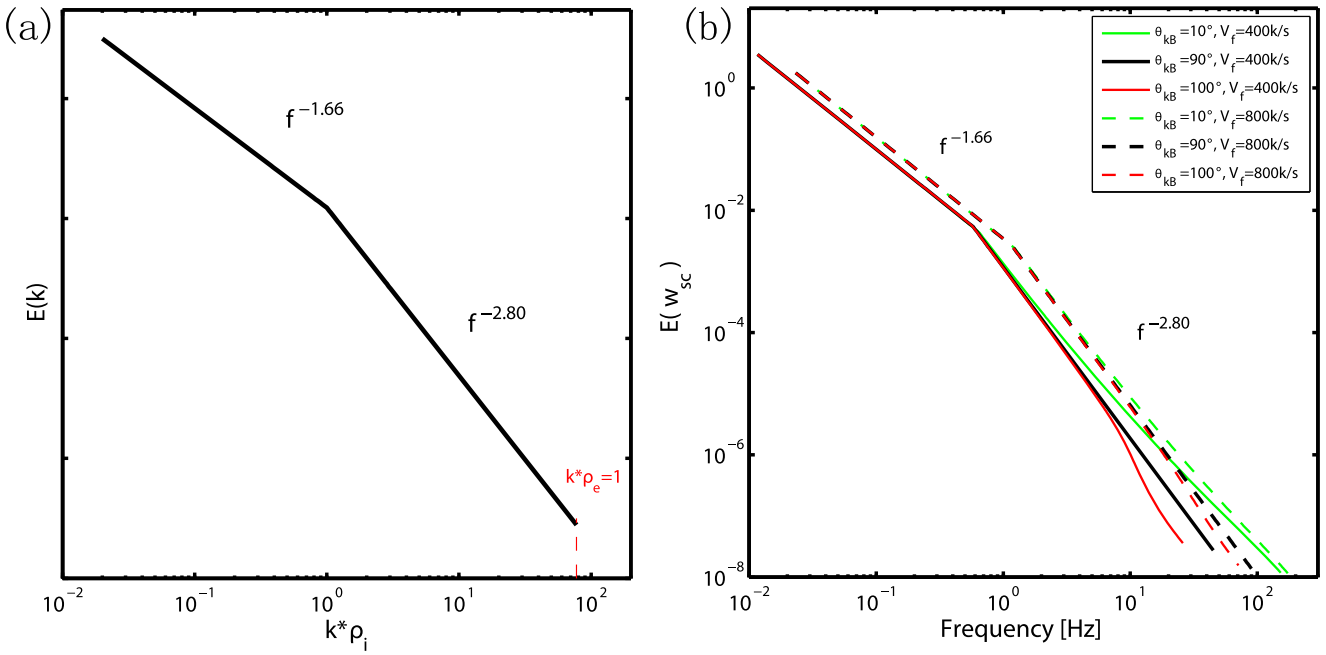

Figure 3. The initial wavenumber spectrum (a) and its transformation in the spacecraft frame for different propagation angles and plasma flow velocities (b).

scales in solar wind turbulence, it can be questionable when it comes to analyzing high-frequency (sub-ion) scales where the phase speeds of the dominant fluctuations (KAW and whistlers) can increase as a function of k and become comparable or larger than the flow speed V (Sahraoui et al. 2012), thus violating the Taylor assumption (Huang & Sahraoui 2019).

Therefore, a legitimate question to ask is: how would the frequency spectra of turbulence measured on board the spacecraft be changed when the two terms on the right-hand side of Equation (1) become comparable?

To answer this question we build a toy model based on the dispersion relation given by Equation (2); (Saito et al. 2010), which mimics that of the (fast) magnetosonic-whistler mode at smaller propagation angles and that of the KAW at high oblique angles at high frequency ($\omega \gtrsim \omega_{ci}$), as derived from the two-fluid theory for $\beta \gtrsim 1$. More details on the properties of these modes can be found in Sahraoui et al. (2012).

$$\omega_{plas} = \frac{k^2 \cos\theta_{\boldsymbol{kB}} d_e^2}{1 + (1 + \sqrt{\beta_e}) k^2 d_e^2} \omega_{ce} \tag{2}$$

Here, $\theta_{\boldsymbol{kB}}$ is the angle formed by the wavevector $\boldsymbol{k}$ and the ambient magnetic field $\boldsymbol{B}$, and d_e, β_e, and ω_{ce} are the electron inertial length, beta, and cyclotron frequency, respectively. Figure 2 shows that, for $\omega \gtrsim \omega_{ci}$, the solution of Equation (2) is very close to the fast mode dispersion relation calculated from the two-fluid theory for $\theta_{\boldsymbol{kB}} = 10°$ and approaches the Alfvén (or intermediate) dispersion at high oblique propagation angle, $\theta_{\boldsymbol{kB}} = 89°$.

To study the impact of the dispersion and the Doppler shift on the spectral slopes we assume an isotropic turbulent spectrum in the wavevector space that has a power law $k^{-1.66}$ in the inertial range and a $k^{-2.80}$ law between ion and electron scales, as featured in Figure 3(a).

Using Equations (1) and (2), we can transform the input spectrum (in wavevector space) into a frequency spectrum as it would be measured on board the spacecraft. Energy conservation imposes

$$E(\omega_{sc}) = E(k)/(\partial\omega_{sc}/\partial k) \tag{3}$$

where $\partial\omega_{sc}/\partial k$ can be determined from Equations (1) and (2). Note that the assumption of an isotropic spectrum imposes that the derivative applies only with respect to $k = |\boldsymbol{k}|$.

3. Results

We start by showing the spectra in the frequency domain resulting from shifting the initial double power-law spectrum using Equations (1)–(3) for three different propagation angles 10°, 90°, and 100° and two flow speeds, $V = 400$ km s^{-1} and $V = 800$ km s^{-1} (for simplicity, we assume a constant angle $\theta_{\mathbf{kV}} \sim 45°$). We use typical plasma conditions in the solar wind to compute the numerical solutions of Equations (1)–(3): $B \sim 10$ nT, $n \sim 15$ cm^{-3}, $T_i \sim 30$ eV, $T_e \sim 10$ eV, yielding $\beta_i \sim 2.3$ and $\beta_e \sim 0.7$. The resulting spectra are shown in Figure 3(b). For $\theta_{\boldsymbol{kB}} \sim 90°$, $\omega_{plas} < \boldsymbol{k} \cdot \boldsymbol{V}$, i.e., the optimum conditions for the Taylor hypothesis to be valid, the frequency spectrum follows the same power law as the wavenumber one (black curves). For $\theta_{\boldsymbol{kB}} = 10°$, the frequency spectra (green curves) become shallower, in particular at high frequencies (Klein et al 2014). Interestingly, for $\theta_{\boldsymbol{kB}} = 100°$, the frequency spectrum (solid red curve) shifts to low frequency and becomes steeper above a new spectral break appearing at intermediate frequencies ~10 Hz. No major changes are seen in the inertial range apart from shifting the ion spectral break toward high frequencies for high flow speeds. This first test shows that fluctuations in the propagation angle and flow speed induce variability in the spectral slopes in the dispersive range while, expectedly, they do not generate any noticeable change in the inertial range (Bourouaine & Perez 2018). Note that the slight broadening in the inertial range comes from the quadratic k dependence of the dispersion relation in Equation (2) in the large-scale limit:

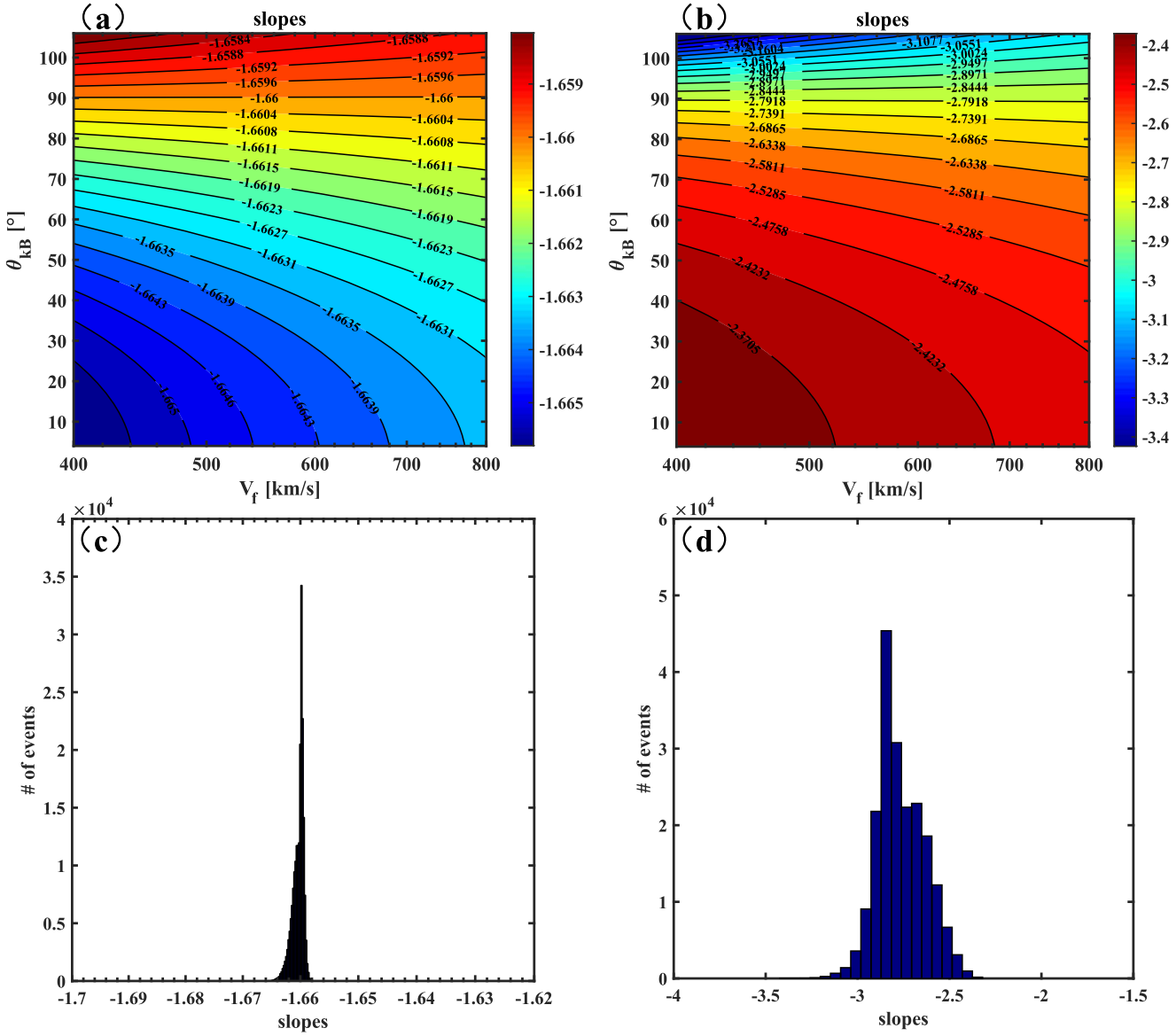

Figure 4. Variability in the spectral slopes (color bar) as function of the propagation angle and the flow speed in the inertial range (a) and the dispersive range (b). The corresponding histograms are shown in (c) and (d), respectively.

$kd_e \ll 1 \Rightarrow \omega \propto k_\parallel V_A k d_i$, which reflects the ion scale correction to the classical (MHD) Alfvén wave dispersion.

The previous study can be generalized to a wider range of propagation angles $\theta_{\boldsymbol{kB}}$ and flow speeds V sampled randomly. The resulting frequency spectra can be divided into three frequency ranges that have different scalings and whose limits are given by the solutions of the equation $\partial^2\omega_{sc}/\partial k^2 = 0$. In this study, we consider only the inertial and dispersive ranges and ignore the third range appearing above the new spectral break seen in Figure 3(b). The results are shown in Figure 4 for $\theta_{\boldsymbol{kB}} \in [4°, 106°]$ and $V \in [400, 800]$ km s^{-1}. We observe that the frequency spectra in the dispersive range become steeper than the input spectrum $k^{-2.8}$ in particular at oblique propagation angles and slow winds, while they are shallower for quasi-parallel to moderately oblique angles. Interestingly, the resulting distribution of the spectral slopes in the dispersive range (Figure 4(d)) reproduces quite well the reported observations from the solar wind (Figure 1(b)). That said, no significant broadening of the slopes distribution around the input value $\alpha = -1.66$ is observed in the inertial range (Figure 4(c)).

Figures 5(a) and (b) show the relative importance of the dispersive effects with respect to the Doppler shift for different propagation angles and flow speeds. While the ratio $\omega_{plas}/\boldsymbol{k}\cdot\boldsymbol{V}$ remains small ($\lesssim$0.1) in the inertial range, it can reach values as high as 2.5 in the dispersive range in particular for slow winds and quasi-parallel propagation, conditions for which the Taylor hypothesis is violated (Howes et al. 2014; Perri et al. 2017; Huang & Sahraoui 2019). If the threshold for the validity of the Taylor hypothesis is set to $\omega_{plas}/\boldsymbol{k}\cdot\boldsymbol{V} \lesssim 0.3$, even propagation angles as high as 80° would violate that assumption. Figures 5(c) and (d) show the resulting spectral slopes as function of the ratio $\omega_{plas}/\boldsymbol{k}\cdot\boldsymbol{V}$. The main observation is that relatively moderate ratios of the dispersive effects to the Doppler shift, typically $\omega_{plas}/\boldsymbol{k}\cdot\boldsymbol{V} \lesssim 1$, produce the bulk of the distribution of the spectral slopes in the dispersive range of solar wind turbulence.

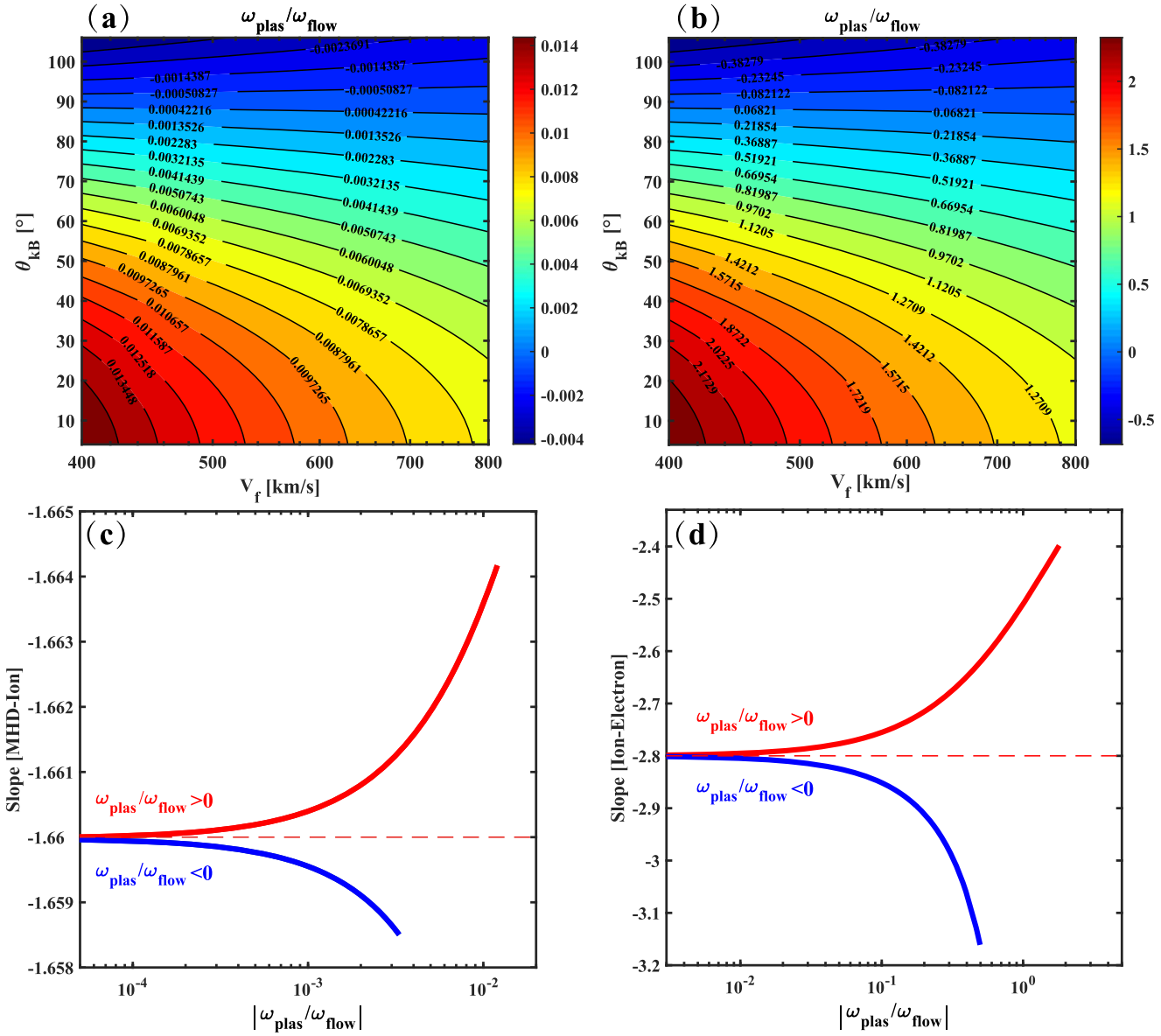

Figure 5. The ratio $\omega_{plas}/\boldsymbol{k}\cdot\boldsymbol{V}$ (color bar) is shown as a function of the propagation angle and the flow speed in the inertial range (a) and the dispersive range (b). The spectral slopes in the inertial range (c) and dispersive range (d) are shown as a function of the ratio $|\omega_{plas}/\boldsymbol{k}\cdot\boldsymbol{V}|$. The red (blue) color indicates positive (negative) values of $\omega_{plas}/\boldsymbol{k}\cdot\boldsymbol{V}$.

4. Discussion and Conclusions

The main conclusion of this study is rather simple: the observed variability of the spectral slopes in the dispersive range of solar wind turbulence can be caused by fluctuations in the flow speed and the propagation angles. The latter can stem from at least two origins: (1) the intrinsic variation of the turbulence spatial anisotropy or the strength of the nonlinearities (given by the parameter $\chi = \frac{k_\perp \delta B}{k_\parallel B_0}$ in Alfvénic MHD turbulence); (2) the variation of the angle $\theta_{\boldsymbol{VB}}$ that actually controls the sampled direction of the turbulence when the Taylor hypothesis is used in spacecraft data analysis (i.e., $\theta_{\boldsymbol{VB}} \sim 0^\circ \rightarrow k_\parallel$, $\theta_{\boldsymbol{VB}} \sim 90^\circ \rightarrow k_\perp$). In other words: even if turbulence had a universal power-law scaling $k^{-2.8}$ in the dispersion range, it is possible this can never be demonstrated as such using single spacecraft data because of the potential competition between the Doppler shift and dispersive effects.

The impact of the dispersive effects, or its corollary the violation of the Taylor hypothesis, on the spectral slopes as illustrated in this study should be kept in mind when analyzing solar-wind observations from single spacecraft data. This is relevant to the ongoing interesting studies based on PSP and Solar Orbiter data (e.g., Bourouaine & Perez 2020; Perez et al. 2021), in particular those looking at the radial evolution of the spectral indices of turbulence (Chen et al. 2020), and to the proposed future multispacecraft multiscale space missions such as Cross-scale, Debye, and Helioswarm (Schwartz et al. 2009; Verscharen et al. 2021).

The toy model presented here is certainly an oversimplified picture of the actual solar wind turbulence. Yet, it yields convincing results by reproducing the spectral slopes observed in the solar wind. It can however be improved in several ways, e.g., by varying the angle $\theta_{\boldsymbol{kV}}$ in Equation (1), which is relevant when looking at the radial evolution of the turbulent spectra, or

by considering the full wavevector anisotropy in Equation (3). It can also be extended to electron scales to reproduce (or not) the spectral indices reported in the electron range (Sahraoui et al. 2013; Huang et al. 2014).

Acknowledgments

This work was part of the THESOW project funded by the Agence Nationale de la Recherche (ANR). S. Y. Huang received support from LABEX Plas@Par through a grant managed by the ANR, as part of the program "Investissements d'Avenir" under the reference ANR-11-IDEX-0004-02, and from the National Natural Science Foundation of China under grant No. 41404132. S.Y.H. thanks S. Saito for valuable discussions.

ORCID iDs

Shiyong Huang https://orcid.org/0000-0002-3595-2525

References

Alexandrova, O., Lacombe, C., Mangeney, A., Grappin, R., & Maksimovic, M. 2012, ApJ, 760, 121
Alexandrova, O., Saur, J., Lacombe, C., et al. 2009, PhRvL, 103, 165003
Bale, S. D., Kellogg, P. J., Mozer, F. S., Horbury, T. S., & Rème, H. 2005, PhRvL, 94, 215002
Bavassano, B., Dobrowolny, M., Mariani, F., & Ness, N. F. 1982, JGR, 87, 3617
Bourouaine, S., & Perez, J. C. 2018, ApJ, 858, L20
Bourouaine, S., & Perez, J. C. 2020, ApJ, 893, L32
Bruno, R., & Carbone, V. 2013, LRSP, 10, 2
Bruno, R., Trenchi, D., & D., T. 2014, ApJL, 793, L15
Bruno, R., & Trenchi, L. 2014, ApJL, 787, L24
Chandran, B. D. G. 2018, JPlPh, 84, 905840106
Chen, C. H. K., Bale, S. D., Bonnell, J. W., et al. 2020, ApJS, 246, 53
Chen, C. H. K., Boldyrev, S., Xia, Q., & Perez, J. C. 2013, PhRvL, 110, 225002
Dmitruk, P., & Matthaeus, W. H. 2007, PhRvE, 76, 036305
Dmitruk, P., Mininni, P. D., & Pouquet, A. 2011, PhRvE, 83, 066318
Dudok de Wit, T., Krasnoselskikh, V. V., Agapitov, O., et al. 2022, JGRA, 127, e30018
Gary, S. P., Chang, O., & Wang, J. 2012, ApJ, 755, 142
Goldstein, M. L., Roberts, D. A., & Fitch, C. A. 1994, JGR, 99, 11519
Hadid, S. Y., Sahraoui, F., Kiyani, K., et al. 2015, ApJL, 813, L29
He, J., Tu, C., Marsch, E., & Yao, S. 2012, ApJL, 745, L8
He, J., Wang, L., Tu, C., Marsch, E., & Zong, Q. 2015, ApJL, 800, L31
He, J. S., Marsch, E., Tu, C. Y., et al. 2011, JGRA, 116, A06207
Howes, G. G., Klein, K. G., & TenBarge, J. M. 2014, ApJ, 789, 106
Howes, G. G., TenBarge, J. M., Dorland, W., et al. 2011, PhRvL, 107, 035004
Huang, S. Y., Hadid, L., Sahraoui, F., Yuan, Z. G., & Deng, X. H. 2017, ApJL, 836, L10
Huang, S. Y., & Sahraoui, F. 2019, ApJ, 876, 138
Huang, S. Y., Sahraoui, F., Andrés, N., et al. 2021, ApJL, 909, L7
Huang, S. Y., Sahraoui, F., Deng, X. H., et al. 2014, ApJL, 789, L28
Huang, S. Y., Wang, Q. Y., Sahraoui, F., et al. 2020a, ApJ, 891, 159
Huang, S. Y., Xu, S. B., Zhang, J., et al. 2022, ApJL, 929, L6
Huang, S. Y., Zhang, J., Sahraoui, F., et al. 2020b, ApJL, 897, L3
Iroshnikov, P. S. 1963, AZh, 40, 742
Kiyani, K., Chapman, S., Khotyaintsev, Y., Dunlop, M., & Sahraoui, F. 2009, PhRvL, 103, 075006
Kiyani, K. H., Chapman, S. C., Sahraoui, F., et al. 2013, ApJ, 763, 10
Klein, K. G., G., H. G., & TenBarge, J. M. 2014, ApJL, 790, L20
Kobayashi, S., Sahraoui, F., Passot, T., et al. 2017, ApJ, 839, 122
Kraichnan, R. H. 1965, PhFl, 8, 1385
Kretzschmar, M., Chust, T., Krasnoselskikh, V., et al. 2021, A&A, 656, A24
Kunz, M., Abel, I., Klein, K., & Schekochihin, A. 2018, JPlPh, 84, 715840201
Kunz, M. W., Schekochihin, A. A., & Stone, J. M. 2014, PhRvL, 112, 205003
Leamon, R. J., Matthaeus, W. H., Smith, C. W., & Wong, H. K. 1998, ApJ, 507, L181
Leamon, R. J., Smith, C. W., Ness, N. F., & Wong, H. K. 1999, JGR, 104, 22331
Matteini, L., Stansby, D., Horbury, T. S., & Chen, C. H. K. 2018, ApJ, 869, L32
Matthaeus, W. H., Breech, B., & Dmitruk, P. 2007, ApJ, 657, L121
Meyrand, R., & Galtier, S. 2012, PhRvL, 109, 194501
Meyrand, R., Squire, J., Schekochihin, A., & Dorland, W. 2021, JPlPh, 87, 535870301
Parashar, T. N., Servidio, S., Shay, M. A., Breech, B., & Matthaeus, W. H. 2011, PhPl, 18, 092302
Passot, T., & Sulem, P. L. 2015, ApJL, 812, L37
Passot, T., & Sulem, P. L. 2019, JPlPh, 85, 905850301
Perez, J. C., Bourouaine, S., Chen, C. H. K., & Raouafi, N. E. 2021, A&A, 650, A22
Perri, S., Servidio, S., Vaivads, A., & Valentini, F. 2017, ApJS, 231, 4
Podesta, J. J., & TenBarge, J. M. 2012, JGRA, 117, A10106
Sahraoui, F., Belmont, G., & Goldstein, M. L. 2012, ApJ, 748, 100
Sahraoui, F., Belmont, G., Pinçon, J. L., et al. 2004, AnGeo, 22, 2283
Sahraoui, F., Belmont, G., Rezeau, L., et al. 2006, PhRvL, 96, 075002
Sahraoui, F., Goldstein, M. L., Belmont, G., Canu, P., & Rezeau, L. 2010, PhRvL, 105, 131101
Sahraoui, F., Goldstein, M. L., Robert, P., & Khotyaintsev, Y. V. 2009, PhRvL, 102, 231102
Sahraoui, F., Huang, S. Y., Belmont, G., et al. 2013, ApJ, 777, 15
Saito, S., Gary, S. P., & Narita, Y. 2010, PhPl, 17, 122316
Salem, C. S., Howes, G. G., Sundkvist, D., et al. 2012, ApJL, 745, L9
Schekochihin, A. A., Cowley, S. C., Dorland, W., et al. 2009, ApJS, 182, 310
Schwartz, S. J., Horbury, T., Owen, C., et al. 2009, ExA, 23, 1001
Simon, P., & Sahraoui, F. 2022, PhRvE, 105, 055111
Smith, C. W., Hamilton, K., & Vasquez, B. J. 2006, ApJ, 645, L85
Squire, J., Meyrand, R., Kunz, M. W., et al. 2022, NatAs, 6, 715
Stawicki, O., Gary, S. P., & Li, H. 2001, JGR, 106, 8273
Sulem, P. L., Passot, T., Laveder, D., & Borgogno, D. 2016, ApJ, 818, 66
Tao, C., Sahraoui, F., Fontaine, D., et al. 2015, JGRA, 120, 2477
Velli, M., Grappin, R., & Manegeney, A. 1989, PhRvL, 63, 1807
Verdini, A., Grappin, R., Pinto, R., & Velli, M. 2012, ApJL, 750, L33
Verscharen, D., Wicks, R. T., Alexandrova, O., et al. 2021, ExA, 54, 473
Voitenko, Y., & de Keyser, J. 2011, NPGeo, 18, 587
Wan, M., Matthaeus, W. H., Karimabadi, H., et al. 2012, PhRvL, 109, 195001